Spherical potassium intercalated activated carbon beads for pulverised fuel CO2 post-combustion capture

Article *in* Carbon · November 2015

DOI: 10.1016/j.carbon.2015.06.036

CITATIONS
61

READS
1,838

8 authors, including:

Nannan Sun
Chinese Academy of Sciences
62 PUBLICATIONS **2,814** CITATIONS
SEE PROFILE

Cheng-Gong Sun
University of Nottingham
85 PUBLICATIONS **2,475** CITATIONS
SEE PROFILE

Colin E. Snape
University of Nottingham
558 PUBLICATIONS **17,746** CITATIONS
SEE PROFILE

Yuhan Sun
Chinese Academy of Sciences
953 PUBLICATIONS **32,334** CITATIONS
SEE PROFILE

CARBON 94 (2015) 243–255

Contents lists available at ScienceDirect

CARBON

journal homepage: www.elsevier.com/locate/carbon

Spherical potassium intercalated activated carbon beads for pulverised fuel CO_2 post-combustion capture

Jingjing Liu [a], Nannan Sun [a,c], Chenggong Sun [a,*], Hao Liu [a,*], Colin Snape [a], Kaixi Li [b,*], Wei Wei [c], Yuhan Sun [c]

[a] Faculty of Engineering, The Energy Technologies Building, Jubilee Campus, University of Nottingham, Nottingham NG7 2TU, UK
[b] Institute of Coal Chemistry, Chinese Academy of Sciences, Taiyuan, Shanxi 030001, China
[c] Shanghai Advanced Research Institute, Chinese Academy of Sciences, No. 99 Haike Road, Zhangjiang Hi-Tech Park, Pudong, Shanghai, China

ARTICLE INFO

Article history:
Received 17 March 2015
Received in revised form 15 June 2015
Accepted 16 June 2015
Available online 23 June 2015

ABSTRACT

Spherical carbon beads with a uniform diameter of *ca.* 0.6–0.8 mm and high mechanical strength can be prepared by hydrothermal synthesis. To optimise the performance of these adsorbents for pulverised fuel post-combustion capture, the efficacy of potassium intercalation via a KOH treatment has been investigated, deliberately using nitrogen-free phenolic resin derived activated carbon (AC) beads so that the enhanced CO_2 adsorption achieved by potassium intercalation could be delineated from any other effects. At 25 °C and CO_2 partial pressure of 0.15 bar, the adsorption capacity of K-intercalated ACs nearly doubled from 0.79 mmol/g for the untreated carbons to 1.51 mmol/g whilst the effect on the morphology and mechanical strength is relatively small. It was found that only slightly more than *ca.* 1 wt.% of K is required to give the maximum benefit from intercalation that increases the surface polarity and the affinity towards CO_2. The notably increased CO_2 uptake of the K-AC beads as a result of modest increase in adsorption heat (32–40 kJ/mol compared to 27 kJ/mol for the original AC), coupled with the fast adsorption kinetics, suggest that the overall energy penalty is potentially superior to strongly basic polyethyleneimine and other amine-based solid adsorbent systems for carbon capture.

1. Introduction

The International Energy Agency (IEA) and Intergovernmental Panel on Climate Change (IPCC) have identified carbon capture and storage (CCS) as a critical greenhouse gas reduction solution [1–6]. However, the successful development and deployment of efficient and cost-effective carbon capture technologies plays a decisive role in determining the viability of CCS as a whole because as it stands now, the cost of carbon capture using the state-of-art energy-intensive CO_2 amine scrubbing technology accounts for over 70% of total CCS cost [7,8]. Consequently, alternative capture technologies have been under intensive development over recent years, including advanced solvent scrubbing, oxyfuel combustion, chemical looping combustion, membrane separation and solid adsorbent looping technologies both at low and high temperatures [9]. Of these capture technologies being developed, low temperature solid adsorbents looping technology (SALT) has widely been recognised as having the potential of being viable for post-combustion CO_2 capture (PCC), offering potentially improved process efficiency at significantly reduced energy penalty, lower capital and operational costs and smaller plant footprints. Various solid adsorbents are under investigation such as zeolites, supported/grafted amines, metallic organic frameworks (MOFs), functionalised carbon materials, and calcium or alkali metal based sorbent materials [5,10–17], and some of these solid adsorbent-based capture systems have been demonstrated at varying scales, the largest being the pilot demonstration of dry carbonate sorbent technology for CO_2 capture at Hadong power plant in South Korea [18].

Amongst the most studied materials as candidates for CO_2 adsorption [19,20], carbon-based adsorbents are characterised by the advantages of relatively low cost, ease of regeneration and generally stable cyclic performance. Traditionally, activated carbons are considered as typical physical adsorbents because of their highly developed micro-porosity and large surface area, which leads to the fact that activated carbons can normally only achieve better adsorption capacities at high CO_2 partial pressures, limiting their use for post-combustion capture where CO_2 partial pressure is usually low [21]. In order to enhance the surface affinity of activated carbons towards the acidic CO_2, many investigations have been carried out to modify the chemistry of carbon surface by

* *Corresponding authors.*
E-mail addresses: cheng-gong.sun@nottingham.ac.uk (C. Sun), liu.hao@nottingham.ac.uk (H. Liu), likx@sxicc.ac.cn (K. Li).

http://dx.doi.org/10.1016/j.carbon.2015.06.036
0008-6223/

manipulating either the precursor materials and/or activation methodologies [22–26]. Thermal or thermochemical post-preparation treatment has been investigated as the potential means to introduce different surface functional groups such as basic oxygen functionalities (ketone, pyrone, chromene, *etc.*), nitrogen functional groups (–NH_2–, –CN, pyridinic nitrogen, *etc.*), other heteroatoms or even ionic liquids [27,28]. On the other hand, the thermodynamic and kinetic properties of adsorption also play an important role in determining the ultimate overall performance of activated carbons materials for CO_2 capture [29]. Liu and Wilcox [30,31] evaluated how the realistic surface functional groups effected CO_2 adsorption using plan-wave electronic structure calculations and found that the adsorption thermodynamics and kinetics can be effectively improved via re-addressing the surface chemistries of carbon materials. However, limited decisive progress has been achieved so far in this field.

It is only recently that carbon-based materials with enhanced CO_2 adsorption capacities at relatively low CO_2 pressures (*ca.* 1.0–1.8 mmol/g at 0.15 bar CO_2 and 25 °C) have been reported [32–37]. Most of the adsorbents in these investigations were prepared by involving nitrogen-containing functionalities, and in most cases coupled with chemical activation by potassium hydroxide (KOH) [19,38–41]. These protocols are effective in enhancing CO_2 adsorption capacities, but the samples obtained were typically porous powders with very low bulk densities which will give low CO_2 uptakes on a volumetric basis. Further, for practical applications where either moving or fluidized-bed adsorbers are used for CO_2 capture, these fine powders need to be agglomerated to form pellets or beads with the aid of binders or other additives, which can dramatically reduce the adsorption capacities and kinetic performance. The use of spherical carbon beads with high physical strength avoids this problem where we have reported on their potential for both pre- and post-combustion capture [42] with CO_2 uptakes at 1 bar being similar to those of many other carbons [43–45]. However, attempts to significantly increase CO_2 uptakes, both by using nitrogen precursors and post-treatment with ammonia, have met with limited success [46–48].

Although the basis to enhance CO_2 uptakes at relatively low partial pressures on carbon-based adsorbents has been established using KOH activation [49,50], only powdered samples have been reported. In this study, the use of potassium (K) intercalation via mild KOH activation as an effective means to boost the adsorption performance of activated carbons for post-combustion CO_2 capture has been investigated, using activated-carbon beads with desirable spherical diameters (*ca.* 0.6–0.8 mm) suitable for direct practical applications. It is noteworthy that the KOH/AC mass ratios we used are much lower (from 0.1:1 to 1:1) than those used in typical standard KOH activations (often 2:1 or even higher [41,51]). The novelty of this study lies in that the potentially vital role of alkaline metal intercalation as a means to enhance the CO_2 adsorption capacity and strength of carbons have been investigated and sufficiently strong K-AC beads suitable for use in practical applications are obtained for the first time, with the beneficial effects of K-intercalation being quantified free from potential interference from nitrogen functionalities by using a phenolic resin as the precursor and, finally, the minimum amount of K required to enhance CO_2 adsorption at a partial pressure of 0.15 bar CO_2 is identified to simulate PCC in pulverised fuel (PF) power plant.

2. Experimental

2.1. Preparation of the raw activated carbon (AC) beads

The AC beads using phenolic resins as precursor were synthesised with a hydrothermal method which has been described elsewhere [42]. Briefly, a solution of hexamethylenetetramine and novolac-type phenolic resins were dissolved in methanol, followed by mixing in aqueous polyvinyl alcohol (PVA), and then the mixture was heated to 130 °C under stirring (400 RPM) in an autoclave for 1 h. After washing with abundant deionised water, the resulted resin beads were dried at 110 °C for overnight before they were carbonised at 830 °C in N_2 for 1 h followed by steam activation for another 1 h at the same temperature to obtain the parent raw AC beads (denoted as PR0).

2.2. KOH treatment

5 g of the raw AC beads were impregnated with 50 ml aqueous solution of KOH for 24 h. After drying in a vacuum oven at 70 °C for overnight, which ensures that all the samples were completely evaporated, the samples were heated in a horizontal tube furnace from ambient to a pre-selected treatment temperature at 3 °C/min and maintained at the temperature for an hour. The samples were then washed with deionized water until neutral filtrate was obtained. Different KOH/AC mass ratios for impregnation and various chemical activation temperatures used in the preparation are summarised in Table 1 along with sample designations.

Some of the samples were further treated by exhaustive Soxhlet extraction using de-ionised water to obtain samples with variable contents of intercalated potassium contents (PR3_700_*x*h, where *x* stands for the extraction duration in hours). Detailed procedures of Soxhlet extraction with deionised water include: (1) The extraction thimble which contained the carbon bead sample was loaded into the main chamber of Soxhlet extractor; (2) Connect the Soxhlet exactor with distillation flask and reflux condenser; (3) Heat the distillation flask to 100 °C and maintain at this temperature for different periods of extraction. By controlling the extraction time, carbons containing different levels of intercalated potassium can be obtained in order to evaluate the importance of intercalated potassium at different levels.

2.3. Characterization of the samples

Physical adsorption of N_2 at −196 °C was carried out on a Micromeritics ASAP 2420 analyser. Prior to any measurements, all samples were degased at 120 °C for overnight. The apparent surface area (S_{BET}) was calculated according to the method suggested by Parra et al. [52]. The cumulative pore volumes (V_{total}) were calculated from the amount of nitrogen adsorbed at P/P_0 of *ca.* 0.99, and the average pore volume was calculated by $4V_{total}/S_{BET}$. The micropore volume (V_{micro}) and surface area (S_{micro}) were determined by the *t*-plot method.

Table 1
Preparation conditions and designation of the AC bead samples.

Number	Sample	Initial KOH/AC mass ratio for impregnation	Chemical activation temperature (°C)
1	PR0	0	None
2	PR1_600	0.1:1	600
3	PR1_700	0.1:1	700
4	PR1_800	0.1:1	800
5	PR2_600	0.3:1	600
6	PR2_700	0.3:1	700
7	PR2_800	0.3:1	800
8	PR3_600	0.5:1	600
9	PR3_700	0.5:1	700
10	PR3_800	0.5:1	800
11	PR4_600	1:1	600
12	PR4_700	1:1	700
13	PR4_800	1:1	800

X-ray Fluorescence (XRF) on selected samples was carried out on a Bruker S8 Tiger Spectrometer. Their morphologies were observed on a FEI Quanta 600 Scanning Electron Microscope (SEM) and JEOL 2100F Transmission Electron Microscope (TEM), respectively. The Energy Dispersive X-ray analysis (EDX) software is Esprit 1.9 by Bruker. X-ray Photoelectron Spectroscopy was measured on a Kratos Analytical Ultra-2008 spectrometer, and X-ray Diffraction (XRD) was carried out on a Bruker D8 instrument. To determine the quantity of remaining potassium for K-ACs after washing, the samples were ashed using a thermogravimetric analyser (TGA, Q600, TA instruments; samples were first dehydrated at 120 °C for 20 min, and then heated to 600 °C with a ramping rate of 20 °C/min, followed by an isothermal period for 40 min). The resultant ashes were analysed by an Inductive Coupled Plasma Optical Emission Spectrometer (Perkin-Elmer Optima 33-DV ICP-OES, USA).

2.4. CO_2 adsorption measurements

The CO_2 adsorption isotherms were measured by the same instrument used for physical adsorption of N_2 (Micromeritics ASAP 2420). Similar to the nitrogen adsorption isotherm tests, samples were degased at 120 °C overnight.

CO_2 adsorption of the K-AC beads was also investigated by using a thermogravimetric analyser (TGA, Q500, TA instruments). The sample was first dried at 150 °C in pure N_2 for 45 min to remove any physisorbed moisture and/or CO_2, the temperature was then cooled to the adsorption temperature (25 °C). After the temperature stabilized, a flow of 100 mL min^{-1} of a simulated flue gas containing 15% CO_2 in N_2 was introduced into the sample chamber at the adsorption temperature for 60 min and the sample weight was recorded in order to calculate the CO_2 uptake. After adsorption, the gas atmosphere was switched to N_2 and the temperature was increased to 150 °C at a rate of 30 °C/min to desorb the CO_2. Up to 50 adsorption–desorption cycles were performed to evaluate the stability of the adsorbent samples.

2.5. Heat of adsorption measurements

The heat of adsorption and the specific heat capacity of the K-AC carbon materials were determined using a SENSYS evo TG-DSC instrument (Setaram) under the conditions similar to those used in adsorption tests using a mixture of CO_2 and nitrogen. Since this instrument simultaneously provides mass changes and heat flows, the heat of adsorption can then be deduced in terms of the heat released per mole of CO_2 adsorbed.

2.6. Mechanical strength testing

The mechanical strengths of the samples were measured using a DMAQ800 dynamic mechanical analyser (TA instruments, USA). The dynamic force exerted on the sample allows the change in deformation with temperature to be monitored. Each sample was tested ten times during which one carbon bead was randomly selected every time to ensure the accuracy of the results. The average values for the 10 repeat tests for each sample are reported.

3. Results and discussion

3.1. Characterization of the K-containing activated carbon beads

3.1.1. Chemical composition

Our previous work has already showed that the parent carbon bead sample (PR0) was free from nitrogen (less than 0.01 wt.%) and inorganics, which was expected as the sample was derived from pyrolysis of a phenolic resin containing negligible impurities compared with coal and biomass-derived ACs [42]. Information from XPS, SEM-EDX and XRF on the distribution of the K is presented in SI1 and SI2. XRF indicates that the K-AC samples activated at 700 °C have concentrations of K in the range of 14–22 wt.%. However, XPS data (SI1) suggests that the surface K concentrations are considerably lower, being slightly less than 10 wt.%. This reveals that most of the K has been effectively intercalated within the carbon beads. It was difficult to precisely link the amount of intercalated K with the KOH/carbon mass ratios used in the preparation method as the formation of some crystalline potassium compound clusters on the outer surface of the carbon beads is evident (see Fig. 1). However, it must be stressed that the materials prepared using the same procedure and conditions are fairly reproducible (SI3).

3.1.2. Textural properties

The N_2 adsorption isotherms are illustrated in Fig. 2 and SI4. Despite the small hysteresis loops observed for some of the samples due to the relatively minor development of mesoporous structures, all isotherms can be generally classified as type I according to IUPAC classification [53], suggesting that the spherical carbons are mainly microporous.

Table 2 summarises the specific BET surface areas, pore volumes, microporosities for all the samples derived from N_2 (77 K) adsorption data. The initial AC bead sample (PR0) exhibits a BET surface area of 1128 m^2/g, which is typical for phenolic resin based activated carbons [54,55]. The micropore surface area (S_{micro}) calculated by the *t*-plot method is fairly close to the BET surface area, consistent with the dominant microporosity. However, it is interesting to note that despite prolonged washing with water, considerably lower BET surface areas and total pore volumes were observed for most of the K-ACs, particularly the PR3 series. These results are in sharp contrast to those reported in the literature where enhanced porosity of carbons was obtained via KOH activation [19,41,56]. Therefore, it appears that the carbon matrix structures inherited from the earlier steam activation has been further modified leading to intercalation of K species but with the loss of some microporosity. Previous investigations [19,57–61] have revealed that KOH activation involves a variety of chemical reactions as detailed below, with the significance of the individual reactions varying with temperatures and KOH/carbon mass ratios. During the activation, KOH acts in three simultaneous/consecutive ways: (1) the catalyst to accelerate the gasification reactions which

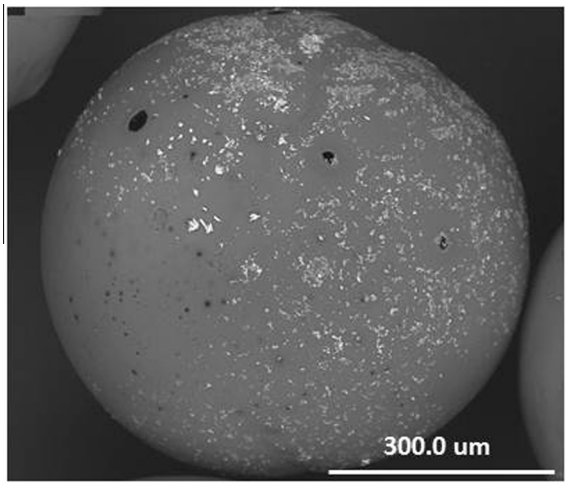

Fig. 1. SEM image of the PR1_700 sample showing the formation of clustered potassium compounds on the outer surface of the treated carbons during the drying process.

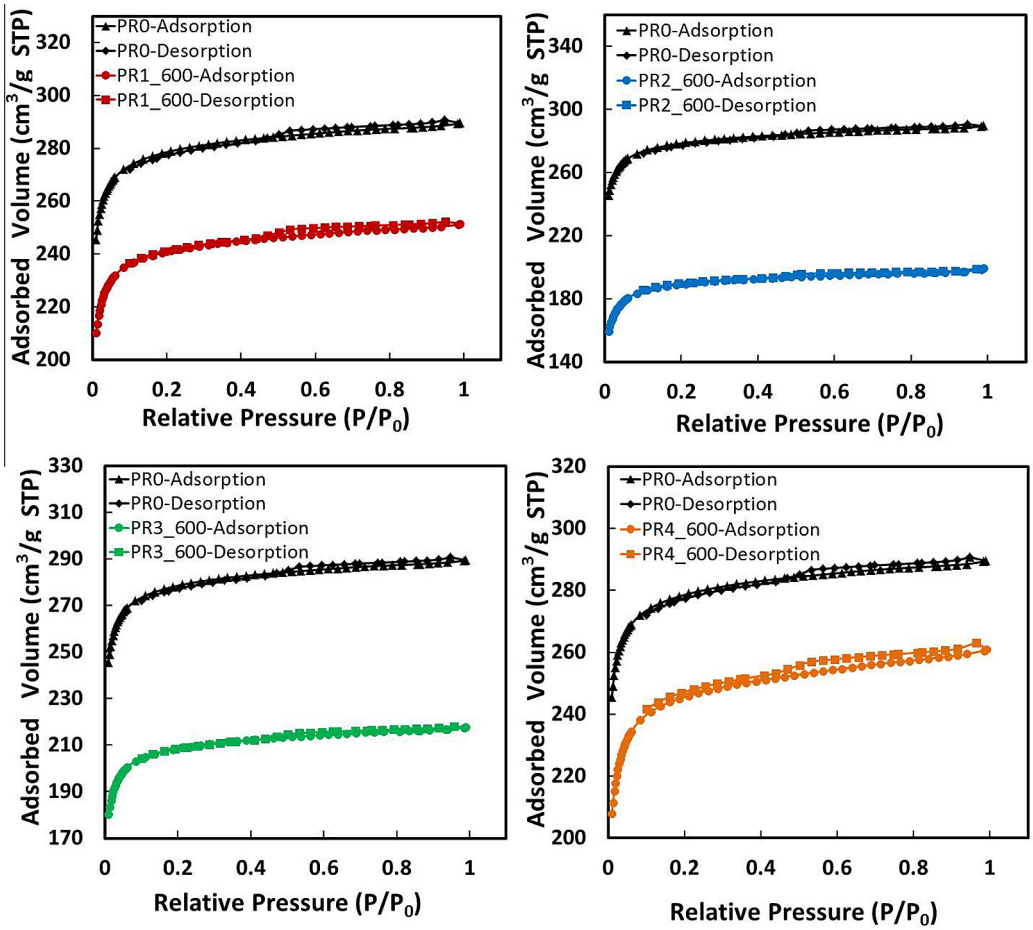

Fig. 2. N_2 isotherms of the raw parent sample PR0 and KOH-intercalated samples PR1_600, PR2_600, PR3_600 and PR4_600. (A color version of this figure can be viewed online.)

Table 2
Texture properties of the carbon beads.

Sample	S_{BET} (m^2/g)	V_{total} (cm^3/g)	Average pore diameter (nm)	S_{micro} (m^2/g)	V_{micro} (cm^3/g)
PR0	1128	0.45	1.59	1115	0.43
PR1_600	972	0.39	1.60	958	0.37
PR1_700	943	0.38	1.61	930	0.36
PR1_800	1047	0.42	1.61	1029	0.40
PR2_600	758	0.31	1.63	748	0.29
PR2_700	902	0.36	1.61	892	0.35
PR2_800	963	0.41	1.70	939	0.38
PR3_600	857	0.35	1.64	843	0.34
PR3_700	826	0.34	1.63	815	0.32
PR3_800	820	0.35	1.69	804	0.32
PR4_600	983	0.40	1.64	963	0.38
PR4_700	1071	0.44	1.65	1050	0.42
PR4_800	1171	0.50	1.76	1150	0.47

are shown in Reactions (1)–(3) and (5). Otowa et al. [61] proposed the reactions of carbon with CO_2 and H_2O (steam) produced from KOH decomposition at temperatures from *ca.* 400 °C, as shown in Reactions (1)–(3). However, recent work by Linares-Solano and his colleagues [56,57,60] has observed that carbon can react directly with KOH as shown in Reaction (5) at temperatures from *ca.* 400 °C as the standard Gibbs free energy of this reaction turns negative from this temperature, and this has been vindicated by the formation of H_2 and K_2CO_3 at temperatures below 700 °C with no appreciable amount of CO and CO_2 being produced [56]; (2) the formation of metallic potassium particularly at temperatures higher than 700 °C that can readily be mobilised and intercalated to the carbon matrix during the porosity development, largely due to the high volatility of metallic potassium (the melting and boiling point for metallic K are 63 and 759 °C, respectively), see in Reactions (5) and (7)–(9); and (3) the formation of potassium carbonate layer as shown in Reactions (4) and (5), which can effectively prevent the carbon from over consumption, although the carbonate can also be partly or wholly consumed in Reactions (6) and (9), depending on the KOH/carbon ratios used. It is believed that the intercalated K is most likely associated with the formed oxygen functionalities (as shown in Reaction (10)) within the carbon matrix structures via the formation of quasi-chemical bonds, giving rise to the residual potassium species that cannot be readily removed by the routine washing with excessive water.

$$2KOH \rightarrow K_2O + H_2O \quad (1)$$
$$C + H_2O(steam) \rightarrow CO + H_2 \quad (2)$$
$$CO + H_2O \rightarrow CO_2 + H_2 \quad (3)$$
$$K_2O + CO_2 \rightarrow K_2CO_3 \quad (4)$$
$$6KOH + 2C \rightarrow 2K + 3H_2 + 2K_2CO_3 \quad (5)$$
$$K_2CO_3 \rightarrow K_2O + CO_2 \quad (6)$$
$$K_2O + H_2 \rightarrow 2K + H_2O \quad (7)$$
$$K_2O + C \rightarrow 2K + CO \quad (8)$$
$$K_2CO_3 + 2C \rightarrow 2K + 3CO \quad (9)$$
$$K_2O + C \rightarrow K + C{-}O{-}K \quad (10)$$

The surface area or microporosity of KOH-activated carbons is determined by a combination of activation temperature and the amount of KOH used. As shown in Table 2, however, the

considerably lower surface areas obtained for most of the samples from the secondary KOH activation of the original steam-activated carbon bead sample (PR0), which has a considerably higher surface area of 1128 $m^2 g^{-1}$, tend to suggest that the potential extra microporosity developed from the secondary KOH activation was offset by the even larger porosity loss as a consequence of the simultaneous potassium intercalation that can potentially lead to complete or partial occlusion of the micropores. It was found that at the same KOH/AC mass ratios, the surface areas of all the K-AC bead samples increased significantly with increasing activation temperatures, highlighting the temperature-dependent reactivity of carbon with KOH. At the same activation temperature, however, the surface areas of the K-ACs were found to decline first with elevating KOH/AC mass ratios from 0.1:1 to 0.5:1 and then increase with further rise in KOH/AC ratios from 0.5:1 to up to 1:1, indicating the relative significance of porosity development and simultaneous potassium intercalation during the chemical activation process.

3.1.3. Morphology

The morphology of the carbon beads was investigated by both SEM and TEM. Fig. 3 shows some of the images from SEM and more can be found in SI5. Fig. 3a–c confirms that the AC samples have well-developed spherical forms with uniform diameters of 0.6–0.8 mm. More importantly, the macroscopic morphology of the samples shows little change after the incorporation of K; the desired spherical form has been preserved. Specifically, cracks and randomly distributed large holes are present on the outer surface. Fig. 3d–f shows the cross-sectional images for the carbon beads where the presence of large number of μm-scale pores and some interior hairline channels are evident. TEM images in Fig. 4 and SI5 reveal the amorphous nano-structures with graphite layers being observed. The fact that no crystallized K species were found reflects their superior uniform distribution, which is of great importance to form highly polarized surfaces to enhance CO_2 capture. This will be further discussed in the following sections.

3.1.4. Element mapping

The distribution of the K species was obtained from SEM element mapping which is depicted in Fig. 5, where red colour represents the existence of K with the brightness indicating concentration. As can be seen from Fig. 5a, no K was detected for the initial AC, PR0, as expected. As shown in Fig. 5b and c, the K-intercalation treatment led to relatively even distributions of K with no obvious segregation, implying that the incorporated K is highly dispersed throughout the carbon beads.

For KOH activated carbons, it is generally recognised that all the residual K species can be removed by subsequent washing with acid (normally HCl solution), by which the porosity in the carbon samples can be recovered [56,62–65]. In the present case, however, deionised water was used as a "soft" washing procedure to successively remove first the "free" and then the intercalated K. In other words, we are attempting to enhance the surface polarity of the carbon beads by potassium intercalation into the carbon frameworks as will be discussed later. Therefore, the distribution of potassium and oxygen on the surface in microscopic scale plays an important role in promoting CO_2 adsorption capacities (Fig. 5). To further investigate the distributions of K and O in relation to C, TEM mapping was carried out, and the results (Fig. 6) suggest that the C, K and O elements are evenly distributed and appear to be interlinked to each other, which confirms that the surface modification is achieved successfully. The high distribution of potassium species can also be evidenced by the weak diffraction peak in the XRD pattern (SI6).

As mentioned above in Section 3.1.2, according to the chemical reactions between C and KOH during the chemical activation, metallic K and quasi-chemical bonds of C–O–K as new surface functionalities can be formed at over 700 °C and efficiently intercalated into the carbon framework structures. When washing with excessive water, most of free surface potassium species, such as K_2CO_3 and K_2O formed during the activation at high temperatures, can be readily removed while intercalated potassium species or related functionalities (e.g. the –O–K chemical or quasi chemical bonds) remain in the carbon matrix structures. The element mapping shown in Fig. 6 illustrates a high consistency between the surface distributions of K and O, further suggesting that the intercalated K is most likely associated with the formed oxygen functionalities via the formation of quasi-chemical bonds, giving rise to highly polarized carbon surfaces.

3.2. CO_2 adsorption on the carbon beads

3.2.1. Static adsorption measurement

As the most used method for adsorbent evaluation, the CO_2 isotherms of the carbon beads were measured both at 0 and 25 °C by a Sieverts apparatus (volumetric method) to obtain the CO_2 adsorption capacities. According to Myers and others [66,67], absolute loadings are needed for thermodynamic processing such as isotherm fitting and adsorption enthalpy calculation, therefore the obtained excessive CO_2 uptakes were converted to absolute uptakes by using Peng–Robinson equation of state (SI7) [68,69], and some of the results are presented in Fig. 7 while the others are provided in the Supporting information (SI8).

All samples display type I isotherms for CO_2 adsorption with a sharp uptake at the early adsorption stage in the low relative pressure region, suggesting that these carbon beads are mainly microporous materials. At atmospheric pressure, sample PR0 adsorbs 4.45 and 2.80 mmol CO_2/g at 0 and 25 °C, respectively, being consistent with those reported elsewhere for phenolic resin derived carbons not modified by nitrogen treatments [42]. For better comparison, the CO_2 adsorption capacities measured at different temperatures and partial pressures are summarised in Table 3 while a comparison with those reported in the literatures for KOH activated carbons is presented in Table 4. As expected, all of the KOH-activated carbon bead samples showed substantially higher adsorption capacities at both temperatures, especially at relative low pressures. It was found that at the same activation temperatures, the adsorption capacity of K-ACs ascended with increasing KOH/AC mass ratios used in the chemical activation. However, no obvious correlation was found between the adsorption capacity and the surface area or porosity of the carbon samples derived from different conditions (Table 2), especially at lower CO_2 partial pressures. At 25 °C and a CO_2 partial pressure of 0.15 bar, the original steam-activated sample (PR0), which has the highest surface area of 1128 m^2/g and micropore volume of 0.43 cm^3/g, adsorbed approximately only half of the amount of CO_2 adsorbed by the K-intercalated PR3_700 sample (1.51 mmol/g), which has a considerably lower surface area of 826 m^2/g and micropore volume of 0.32 cm^3/g, highlighting the importance of potassium intercalation for enhanced CO_2 adsorption performance of the carbons. Similar phenomenon was also observed for the K-AC samples. For each series of samples obtained from using the same KOH/AC ratios in activation, the adsorption capacity of the activated samples at 800 °C was found to be considerably lower than that of the samples activated at 700 °C, despite the higher surface areas of the activated samples at the higher activation temperatures. For all the KOH/AC mass ratios examined, the K-AC samples activated at 700 °C exhibit the best performance for CO_2 uptake.

Although carbon beads derived from a nitrogen-free phenolic resin was deliberately used in this study in order to eliminate the effects of any other heteroatoms in the precursors, a comparison of the K-ACs with the nitrogen-enriched carbons reported in

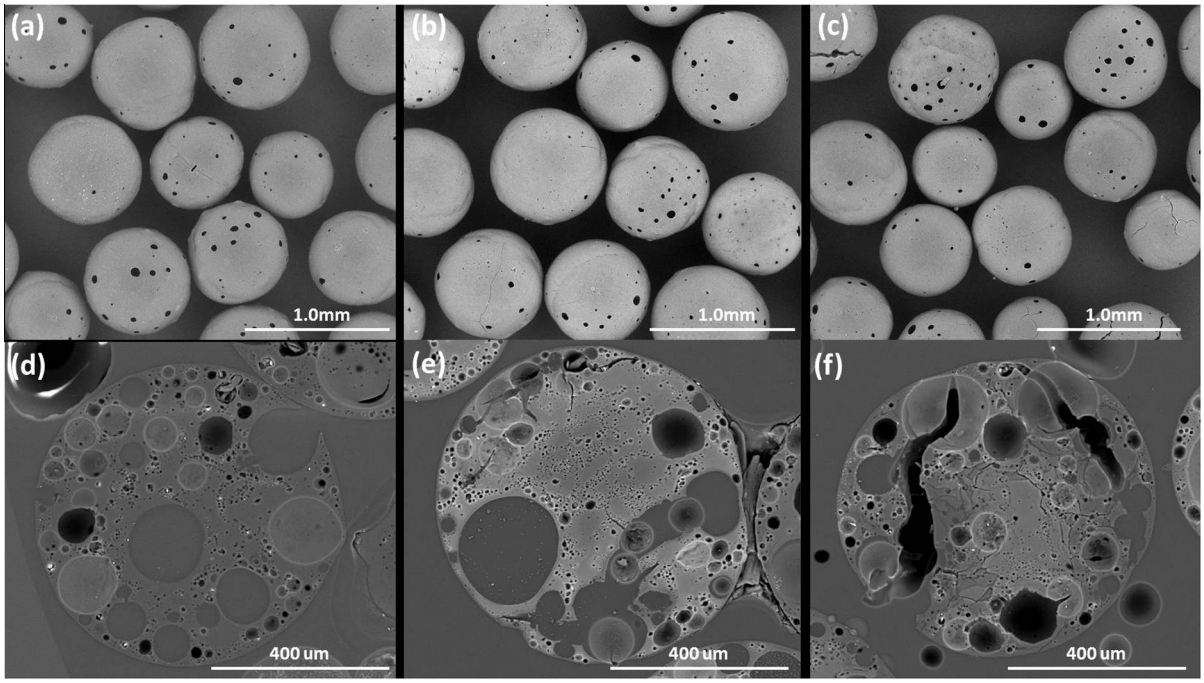

Fig. 3. SEM images of (a) original PR0, (b) PR3_700 (KOH/AC mass ratio of 0.5:1), (c) PR4_700 (KOH/AC mass ratio of 1:1), and their corresponding cross-sectional images (d–f).

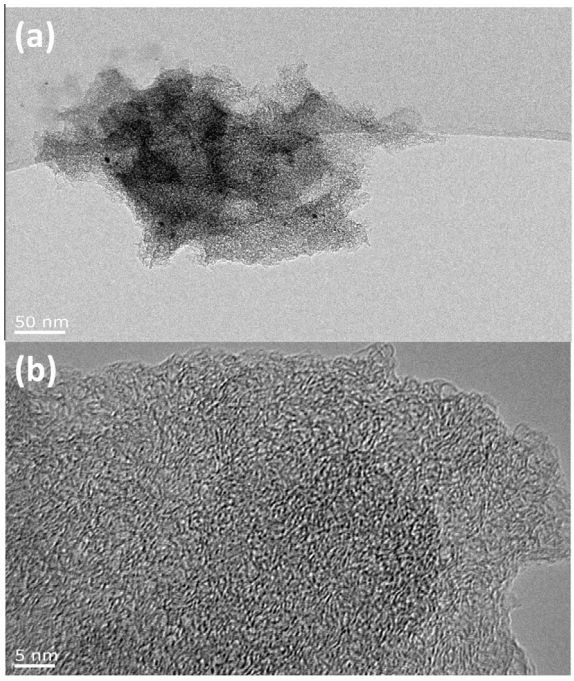

Fig. 4. High resolution TEM images of the activated carbon beads (sample PR3_700).

the literature (Table 4) shows that the CO_2 adsorption capacities of our K-AC samples are overall comparable to the nitrogen-enriched carbons reported in literature, despite their significantly lower surface areas (hence potentially higher capacities on a volumetric basis) and the absence of nitrogen functionalities (Tables 1, 2 and 4). More importantly, all the K-AC beads were measured as produced with desirable spherical diameters typically varying between 0.6 and 0.8 mm.

As already been described that although various AC adsorbents have been reported with high CO_2 adsorption capacities, most of the reported carbons were produced in powder forms via processes that often require sophisticated post-treatments, such as HNO_3 oxidation and/or NH_3 activation, leading to significantly increased production costs and reduced carbon yields. Further, carbons produced in fine powder forms cannot usually be used in moving-bed or fluidized bed reactors and will have to be further engineered via pelletisation or granulation to form different types of shapes with required particle sizes, and this can sharply reduce the adsorption capacity and kinetics of the carbon adsorbents [42].

As indicated in Table 5, the K intercalation treatment as a means to improve adsorption performance only has a relatively small impact on the mechanical strength of the carbon beads. The addition of 0.1 and 0.3 KOH mass ratio to the carbon beads only reduces the mechanical strength by *ca.* 10 and 20%, respectively. This reduction is easily tolerated for fluidised bed operation given the high mechanical strength of the initial beads.

One should also bear in mind that while the adsorption capacity on a weight basis is important in terms of the scale-up of the adsorption-based CO_2 capture process, the form and density of the activated carbons will also be critical, with the adsorption capacity on a volumetric basis instead ultimately determining the size and process efficiency of the adsorbent bed. Therefore, it is evident that the overall performance of the adsorbents will be a compromise between adsorbent materials having high surface area and micro-porosity while having sufficient density to maximize the volumetric adsorption capacity. To this end, the phenolic resin derived activated carbon beads from the present study are highly advantageous over the reported carbons, given their significantly lower porosity, higher bulk density (0.39 g/cm^3) and much easier-to-handle spherical forms with practical diameters. Scaled-up production of these novel carbon bead adsorbents is underway in order to further evaluate their performance for CO_2 capture on a volumetric basis using a kg-adsorbent scale fluidized bed reactor [71].

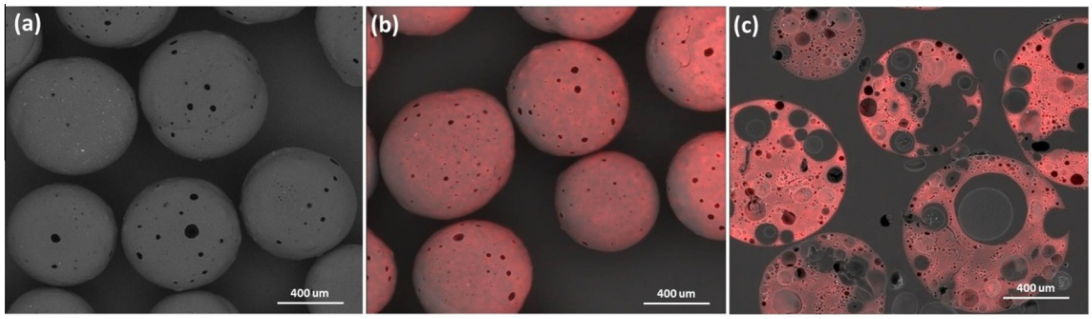

Fig. 5. SEM images of potassium mapping: (a) sample PR0, (b) sample PR3_700, (c) cross-section of sample PR3_700. (A color version of this figure can be viewed online.)

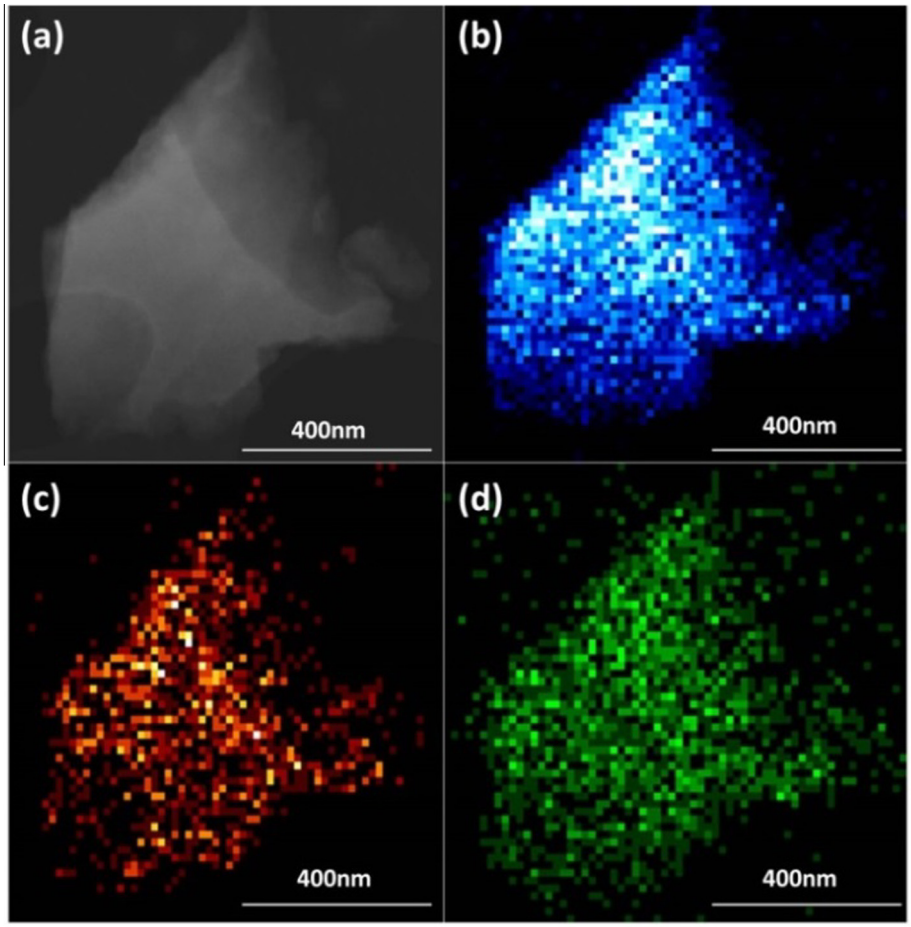

Fig. 6. TEM images of PR3_700, showing the distribution of different elements: (a) original image, (b) carbon mapping, (c) potassium mapping, (d) oxygen mapping. (A color version of this figure can be viewed online.)

3.2.2. Heat of adsorption

Heat of adsorption is an important thermodynamic parameter for describing the adsorption behaviour of an adsorbent and evaluating the energy performance of a process of adsorption and desorption, such as the pressure swing and temperature swing gas separations. Isosteric heat of adsorption (Q_{st}) can be used to indicate the surface affinity of an adsorbent towards an adsorbate. It is usually estimated by using the Clausius–Clapeyron Eq. (1):

$$Q_{st} = -RT^2 \left[\frac{\partial \ln P}{\partial T}\right]_q \quad (1)$$

where R represents specific gas constant; q stands for the adsorption capacity and T, P is the temperature and pressure, respectively. By fitting the obtained experimental isotherms at different temperatures with isotherms equations, one can acquire the pressure (P) needed to reach the same adsorption capacity (q) at different temperatures (T), and then Q_{st} can be calculated by fitting the Clausius–Clapeyron equation.

In this work, the dual-site Langmuir (DSL) equation was used to fit the adsorption isotherms of all K-AC samples as the one-site Langmuir equation is no longer adoptable due to the surface heterogeneity of the carbon surface as a result of potassium intercalation [72,73]. Indeed, recent investigations have proposed that DSL equation is a better model to fit the adsorption isotherms of carbons with high surface heterogeneity [74,75]. The DSL Eq. (2) can be expressed as follows:

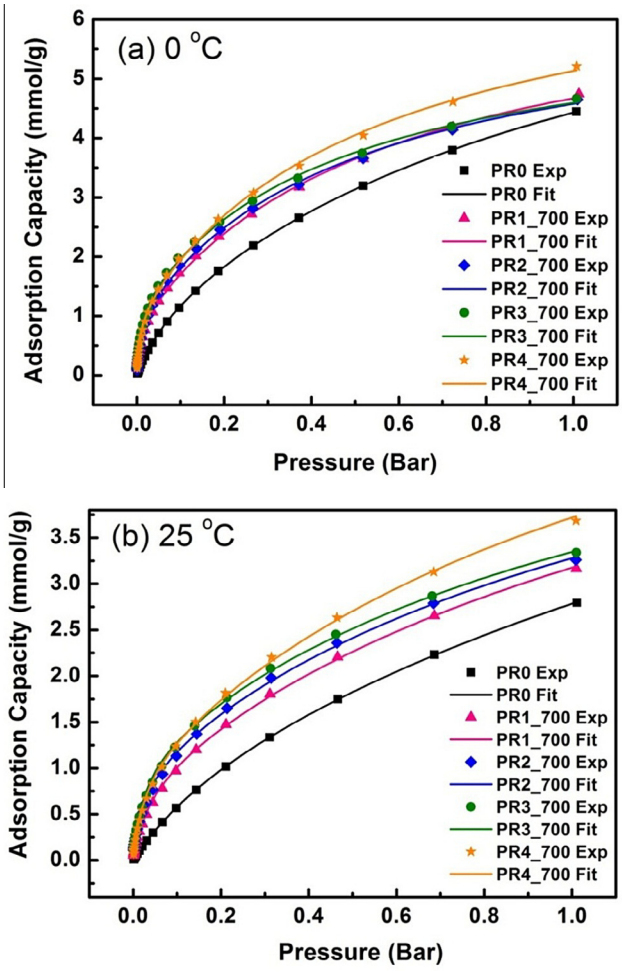

Fig. 7. CO_2 adsorption isotherms of the carbon beads at 0 °C and 25 °C (symbols represent the measured values and lines are the fitted values with the dual-site Langmuir isotherm equation). (A color version of this figure can be viewed online.)

$$q = \frac{q_{s,A} \times b_A \times P}{1 + b_A \times P} + \frac{q_{s,B} \times b_B \times P}{1 + b_B \times P} \quad (2)$$

where $q_{S,A}$ and $q_{S,B}$ are the mono-layer capacity of site A and B, b_A and b_B are the adsorption equilibrium constants for site A and B. During the fitting of isotherms, one must note [76]:

(1) use absolute adsorption capacities;

(2) $q_{S,A}$ and $q_{S,B}$ should be kept constant at all temperatures to fulfil their physical meanings;

(3) b_X (X = A or B) usually decreases with increasing adsorption temperature and is related to a temperature-independent constant, $b_{0,x}$ by the Arrhenius Eq. (3).

$$b = b_0 exp\left(\frac{E}{RT}\right) \quad (3)$$

In Eq. (3), E can be used to indicate the average adsorption heat. Since the fitted isosteric heat of adsorption was obtained as a function of adsorbed CO_2 in which case Q_{st} represents the average of all adsorption sites that can be potentially occupied at a certain coverage level [77,78], the calculated heat of adsorption corresponds to the values at initial coverage (at a CO_2 uptake level of 0.01 mmol/g). However, it is noteworthy that the calculated adsorption heat may differ from the isosteric heat (Q_{st}) of adsorption, but the difference should be quite small [78].

After taking account of these criteria, the experimental isotherms were fitted and some of the fitting curves are shown in Fig. 7 while the others are provided in SI8 and SI9. Fig. 8a illustrates the calculated Q_{st} for both the parent and KOH-intercalated carbon beads at a CO_2 uptake level of 0.01 mmol/g. Generally, a considerable increase in isosteric adsorption heat was observed for all K-intercalated carbon bead samples comparing with the parent carbon beads (PR0). For instance, the calculated isosteric adsorption heat of K-intercalated PR1 and PR3 series carbons increased by up to 60% to *ca.* 36–42 kJ/mol CO_2 from 26 kJ/mol CO_2 for the parent carbon beads (PR0), respectively. This highlights the effectiveness of K intercalation in improving the surface affinity of the carbons for CO_2 adsorption particularly at low CO_2 partial pressures.

Isosteric adsorption heat is also used to indicate the degree of surface heterogeneity of the adsorbent or different interactions between adsorbent and adsorbate. For energetically heterogeneous surfaces, the isosteric heat of adsorption will decrease with increasing quantities of adsorbed substances due to the occurrence of different types of active adsorption sites. Fig. 8b shows the isosteric adsorption heat both for the parent (PR0) and K-intercalated carbons (PR3 series) at different CO_2 uptake levels. The calculated isosteric adsorption heats are by and large close to the upper range of the reported adsorption heats for carbon-based adsorbents [44,79,80]. While higher isosteric adsorption heats were obtained for all K-ACs, the variation of isosteric heat of adsorption with the quantities of CO_2 adsorbed is much higher for the K-ACs than for the initial carbon beads with the isosteric adsorption heat remaining relatively constant. This demonstrates that the porous

Table 3
CO_2 adsorption capacities of the carbon beads.

Sample	CO_2 capacity at 0 °C (mmol/g)		CO_2 capacity at 25 °C (mmol/g)	
	0.15 bar	1 bar	0.15 bar	1 bar
PR0	1.52	4.43	0.79	2.78
PR1_600	1.92	4.45	1.14	3.02
PR1_700	2.07	4.67	1.23	3.17
PR1_800	2.06	4.74	1.26	3.27
PR2_600	2.06	3.95	1.38	2.97
PR2_700	2.19	4.58	1.40	3.28
PR2_800	1.83	4.25	1.12	2.91
PR3_600	2.18	4.29	1.43	3.18
PR3_700	2.33	4.59	1.51	3.35
PR3_800	1.95	4.25	1.23	3.06
PR4_600	2.16	4.68	1.36	3.35
PR4_700	2.35	5.13	1.52	3.72
PR4_800	2.00	5.07	1.25	3.47

Table 4
Comparison on the adsorption capacities of PR3_700 and other carbon adsorbents.

Materials	Precursor	S_{BET} (m^2/g)	Uptake at 25 °C* (mmol/g)		Ref.
			0.15 bar	1 bar	
PC-2	Agaricus	1479	0.88	3.46	[33]
KNC-A-K	P-diaminobenzene	614	1.81	4.04	[36]
IBN9-NCI-A	P-diaminobenzene	890	1.62	4.50	[70]
VR-93	Vacuum residue	2895	1.02	4.83	[32]
CEM-750	N-doping carbon	3360	0.98	4.38	[34]
RFL-500	Resorcinol, formaldehyde and lysine	467	1.50	3.21	[46]
CSA-700	Poly (acrylonitrile-co-acrylamide)	1231	2.11	3.80	[37]
PR3_700	Phenolic resin	826	1.51	3.35	This work

* All results are measured by static volumetric method.

Table 5
Mechanical strength of K-ACs (activated at 700 °C).

Sample	KOH/AC mass ratio	Maximum load (N)
PR0	0	3.08
PR1_700	0.1:1	2.86
PR2_700	0.3:1	2.47
PR3_700	0.5:1	2.21
PR4_700	1:1	1.75

surface of the K-intercalated carbons becomes energetically much more heterogeneous, being indicative of the incorporation of new active adsorption sites (Fig. 6) that led to higher interaction energy of CO_2 with the surface.

In order to validate the calculated isosteric heat of adsorption with the dual-site Langmuir model, TGA-DSC has been used to experimentally measure the adsorption heat of the carbon beads. Given that the measured value by TGA-DSC represents the averaged adsorption heat integrated from the DSC heat flow corresponding to the adsorption capacity of a carbon adsorbent, the following Eq. (4) [81] was used to derive the integral adsorption heat values from the isosteric heat of adsorption. The integral adsorption values correspond to the defined ranges of sorption-phase concentration from 0 to n, where n equals to the equilibrium CO_2 adsorption capacity obtained by TGA-DSC in a calorimetric analysis.

$$Q_{int} = \frac{1}{n}\int_0^n Q_{st}\,dn \tag{4}$$

The calculated adsorption heat was then validated by the adsorption heat experimentally measured by TGA-DSC. As shown in Table 6, for the original steam-activated carbon bead sample, the measured and calculated adsorption heats for the original steam-activated carbon beads are almost identical while for the K-intercalated carbons, the calculated adsorption heat values appears to be slightly lower by 1–6 kJ/mol CO_2, compared to the values measured by TGA-DSC. The good agreement obtained between the calculated and measured adsorption heat for most of the carbon bead samples confirms the suitability of the DSL modelling for evaluating the adsorption behaviour of surface-modified carbons.

3.3. The role of intercalated potassium in CO_2 adsorption

The results in the previous sections demonstrate that K intercalation can significantly improve the CO_2 adsorption performance of the phenolic resin derived carbon beads. It can be reasonably assumed that the increased CO_2 adsorption capacity arose from either increased micro-porosity or modified surface chemistries or a combination of both. As Table 2 indicates, however, a considerable decrease rather than an increase in surface area and microporosity was observed for all the K intercalated carbon samples under the conditions used, despite the washing with excessive quantities of deionised water. This suggests that the improved CO_2 adsorption of the K-ACs cannot be accounted for by the surface textual properties but by the modified surface chemistries. It has been well established that KOH-activated carbons are usually enriched in different surface oxygen functionalities [82–84], but the presence of the surface functionalities alone is not sufficient to explain the significant increase in CO_2 capacities according to the results reported elsewhere [37,85]. It is therefore considered that the intercalated K is responsible for the enhanced CO_2 adsorption performance of the K-ACs. To provide further insight, an exhaustive Soxhlet extraction at 100 °C with deionised water as the solvent was used to remove the intercalated potassium in the K-AC samples to different levels. This was used to evaluate the variation of CO_2 adsorption with different levels of potassium intercalation and hence to determine the minimal content of intercalated potassium that is required to achieve appreciable improvement in CO_2 adsorption. One of the K-AC samples, the PR3_700 which exhibited the highest CO_2 capacity at 25 °C and a CO_2 partial pressure of 0.15 bar, was selected for the exhaustive Soxhlet

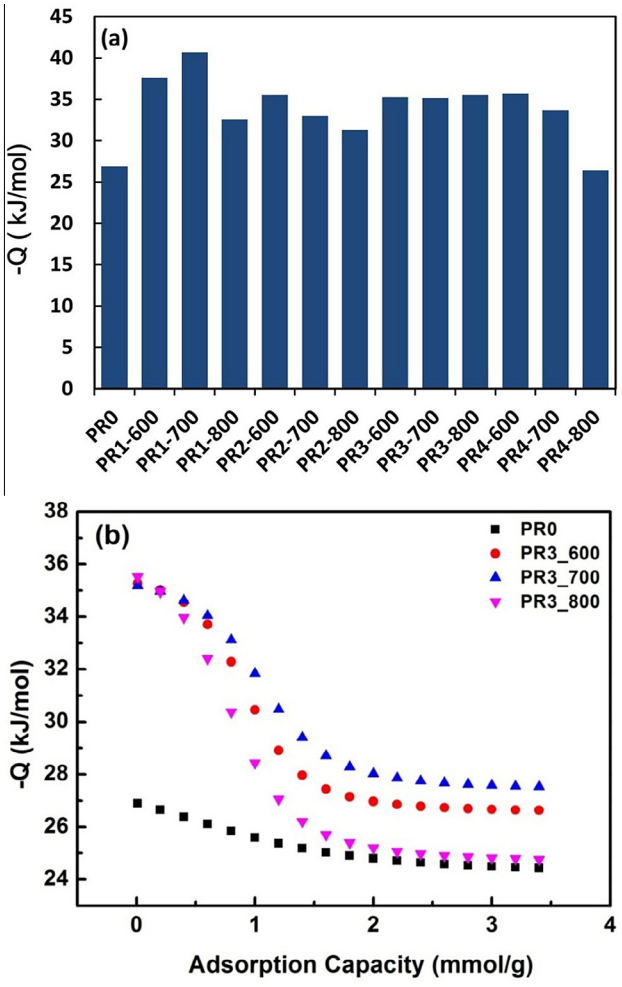

Fig. 8. (a) Fitted isosteric adsorption heat at a CO_2 uptake level of 0.01 mmol/g for all the carbon beads; (b) Fitted isosteric adsorption heat of PR0 and PR3 series as a function of absolute CO_2 loading using dual-site Langmuir model. (A color version of this figure can be viewed online.)

Table 6
Comparison between analytical integral heat of adsorption by DSL model and measured DSC heat of adsorption.

Sample	Analytical integral heat of adsorption by DSL model (kJ/mol)	Experimental measured heat of adsorption by TG-DSC (kJ/mol)
PR0	26.0	26.7
PR1_600	34.1	33.9
PR1_700	36.9	39.7
PR1_800	30.6	33.7
PR2_600	35.6	38.2
PR2_700	31.4	35.1
PR2_800	29.6	33.0
PR3_600	33.3	38.8
PR3_700	33.3	35.5
PR3_800	32.4	34.2
PR4_600	33.2	34.9
PR4_700	31.6	34.6
PR4_800	25.3	31.3

extraction for different extraction times. The samples produced from different periods of extraction were then subjected to CO_2 adsorption tests and other characterisations.

Table 7 summaries the textural properties of the extracted samples and their CO_2 adsorption capacities measured at both 0 and 25 °C and a CO_2 partial pressure of 0.15 bar. As expected, the amount of K present decreased with increasing extraction time and after 20 h extraction, the potassium content was reduced from 9.25% to only 0.57% on a weight basis. As can be seen from Table 7, the BET surface area of the carbon sample increased considerably with increasing removal of the intercalated potassium from the carbons, particularly at the early stages of Soxhlet extraction. This confirms that the lower surface areas obtained for the K-AC samples (Table 2) was due to the potassium intercalation which led to partial or even complete occlusion of micropores.

Measurements of CO_2 adsorption capacity before and after the Soxhlet extraction, presented in Table 7 and Fig. 9, demonstrate that the capacity shows no significant change with decreasing residual potassium content from *ca.* 9.2 to 2.8 wt.%, but a sharp decrease was observed when potassium content was further reduced to below 1 wt.%. It appears that there is a critical concentration of potassium above which the excess residual potassium contributes little to CO_2 adsorption capacity. It can be reasonably assumed that the hard-to extract residual quantities of K are deeply intercalated into the fine carbon structure in the form of extra-framework K^+ cations. Previous investigations [36,86] showed that stronger CO_2 adsorption sites of zeolite, MOF adsorbents reside predominantly around unsaturated framework metal cations. Therefore, it is believed that the significantly improved CO_2 adsorption as a result of the intercalation of K cations is due to the involvement of stronger electrostatic forces created by the exposed framework K^+ ions on the surface, with the strength of the electrostatic interaction being determined by the surface density and nature of the extra-framework K^+ cations, an adsorption mechanism similar to that observed for the MOF-based CO_2 adsorbents [36,86]. Indeed, strong electrostatic properties were observed in handing the K-AC samples which were found to be easily attached to the interior surface of the sample cell and showed appreciable repulsion behaviour between different K-AC carbon beads while similar phenomena were not observed for the parent carbon beads.

It is very likely that the strong electrostatic interaction may lead to the formation of labile carbonate-like complexes upon CO_2 adsorption around the extra-framework cations [87]. As highlighted in the following cyclic adsorption/desorption tests in dry gas conditions, the enhanced CO_2 adsorption of the K-ACs, does not require the participation of water or moisture in the adsorption process unlike the K_2CO_3-based adsorbents where the presence of significant quantities of moisture in the gas stream is essential to the CO_2 adsorption [88].

3.4. Cyclic adsorption/desorption and stability testing of the K-AC adsorbents

Fig. 10 presents the adsorption/desorption characteristics of one of the K/AC samples (PR3_700) obtained from TGA at a temperature of 25 °C and a CO_2 partial pressure of 0.15 bar (N_2 balance). As shown in Fig. 10a, a final equilibrium CO_2 adsorption capacity of 1.9 mmol/g is obtained with approximately 90% of the equilibrium capacity achieved in 5 min under the TGA test conditions. This highlights the high capacity and fast adsorption kinetics of the K-AC beads, although it takes a slightly longer time for the K-ACs to reach equilibrium adsorption compared to the parent ACs. Fig. 10b shows the cyclic adsorption/desorption testing results for the K-AC carbon bead sample. The cyclic life-time performance testing demonstrates the excellent reversible adsorption performance of the K-intercalated carbon beads, despite the slight decrease in CO_2 capacity in the first 5 cycles, which appears to be attributable to the irreversible CO_2 adsorption on non-intercalated potassium species (as shown by bright red spots in Fig. 5b) in the dry flue gas conditions.

Table 7
Characterization results for the extracted samples from PR3_700 (K concentrations determined by ICP).

Sample	S_{BET} ($m^2\ g^{-1}$)	K (wt.%)
PR3_700_1.5 h	892	9.25
PR3_700_2.5 h	984	2.79
PR3_700_4.0 h	1053	0.96
PR3_700_20 h	1074	0.57
PR0	1128	<0.01

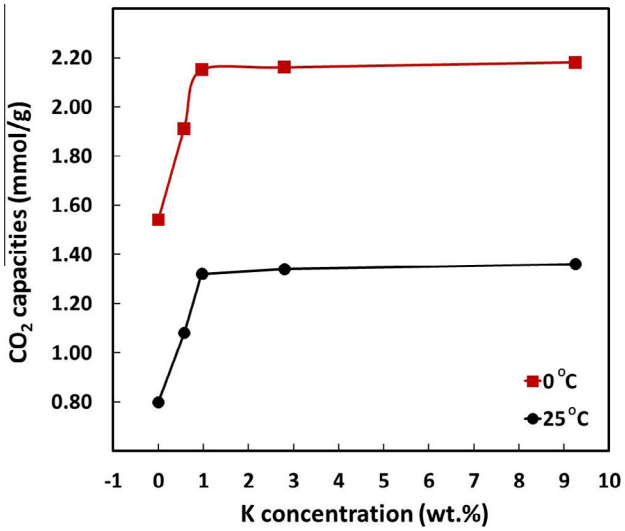

Fig. 9. The influence of K concentration (determined by ICP) on the CO_2 capacities for deionised water extracted samples from PR3_700. (A color version of this figure can be viewed online.)

Apart from overall stability in multi-cycle tests, the regeneration energy needs to be considered in order to evaluate the efficiency and cost-effectiveness of the K-AC samples as CO_2 adsorbents. The required regeneration energy of a solid adsorbent is the sum of the sensible heat that is required to heat the adsorbent from the adsorption temperature to the regeneration temperature and the latent heat (heat of adsorption) that is required to overcome the bonding energy to remove CO_2 from the adsorbent in the desorption process [89]. It has been reported [90] that amine-functionalised solid adsorbents such as PEI-silica generally require less regeneration energy (in a cyclic temperature swing adsorption/regeneration CO_2 capture process) compared with the benchmark MEA scrubbing technology. The facts that the K-AC beads developed in this study have much lower heat of adsorption and specific heat capacity (e.g. 36 kJ/mol, 1.1 kJ/kg.K for PR3_700) than PEI/silica adsorbents (60–90 kJ/mol, 1.7 kJ/kg.K [71,91,92]), comparable CO_2 capacities and superior regenerability indicate that K-AC adsorbents are potentially better alternatives for PEI-silica for PCC in coal-fired PF coal-fired power plants.

4. Conclusions

The use of potassium intercalation via relatively mild KOH activation has been investigated as a novel effective means to boost the adsorption performance of activated carbons for post-combustion carbon capture. A nitrogen-free phenolic resin

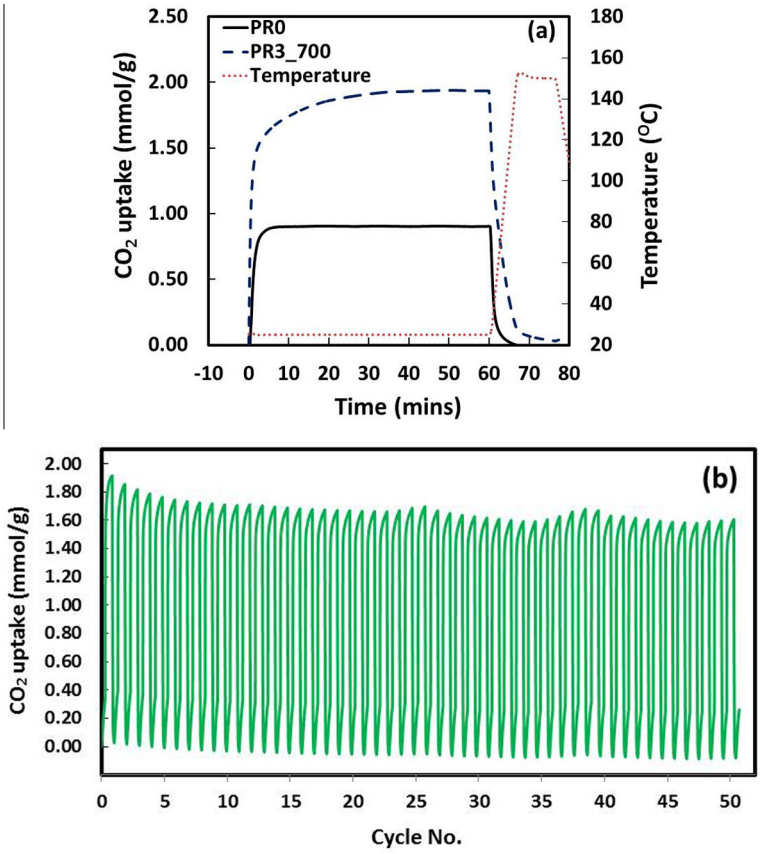

Fig. 10. (a) The CO_2 adsorption curve of PR0 and PR3_700; (b) 50 cycles of the adsorption and desorption for PR3_700; both under an atmosphere of 15% CO_2 and 85% N_2 at 25 °C. (A color version of this figure can be viewed online.)

derived spherical carbon material with desirable spherical diameters (0.6–0.8 mm) which is suitable for direct practical applications without further palletisation or granulation treatment has been used so that the enhanced CO_2 adsorption achieved by potassium intercalation could be delineated from any other effects. The results demonstrated that the intercalation of K significantly increased the CO_2 capacity of the AC beads by a factor of up to 2 at 0.15 bar CO_2 partial pressure while the effects of potassium intercalation on the mechanical strength and morphological features of the carbon beads were negligible at KOH/AC mass ratios of $\leqslant$0.3.

The results suggest that the enhanced CO_2 adsorption of potassium-intercalated carbons, as highlighted by their modestly increased heat of adsorption, is closely related to the formation of carbon framework or extra-framework K^+ cations, which can lead to the potential formation of $K^{\delta+} - O^{\delta-}$ zwitterion-like structures that can boost the electrostatic interaction of the carbon surface with CO_2. In addition, there appears to be a low critical K concentration, which is not much more than *ca.* 1 wt.% in the case of the carbon beads examined, below which the beneficial effect of K intercalation on CO_2 adsorption becomes negligible. The results also demonstrate that the dual-site Langmuir model can be used to effectively characterise the adsorption behaviour of the K-intercalated carbons where high surface heterogeneity exists.

The significantly increased CO_2 adsorption capacity, modest adsorption heat, fast kinetics and good mechanical strength augurs extremely well that the K-AC adsorbents could provide a sound alternative to the most studied polyethyleneimine-based sorbents for improved energy penalty of post-combustion capture using low temperature solid adsorbent looping technology.

Acknowledgements

The authors wish to acknowledge the financial support from the UK EPSRC (Grant nos: EP/G063176/1 and EP/J020745/1) and the National Natural Science Foundation of China (Grant nos: 51061130536, 51172251). The authors also wish to thank Dr. Wenbin Zhang from the University of Nottingham for assisting in the measurements of adsorption heat.

Appendix A. Supplementary data

Supplementary data associated with this article can be found, in the online version, at http://dx.doi.org/10.1016/j.carbon.2015.06.036.

References

[1] M.M. Halmann, M. Steinberg, Greenhouse Gas Carbon Dioxide Mitigation: Science and Technology, CRC Press, 1998.
[2] D.B. Dell'Amico, F. Calderazzo, L. Labella, F. Marchetti, G. Pampaloni, Converting carbon dioxide into carbamato derivatives, Chem. Rev. 103 (10) (2003) 3857–3898.
[3] V. Scott, S. Gilfillan, N. Markusson, H. Chalmers, R.S. Haszeldine, Last chance for carbon capture and storage, Nat. Clim. Change 3 (2) (2013) 105–111.
[4] J.T. Houghton, Y. Ding, D.J. Griggs, M. Noguer, P.J. van der Linden, X. Dai, et al., Climate Change 2001: The Scientific Basis, Cambridge University Press, Cambridge, 2001.
[5] P.H. Stauffer, G.N. Keating, R.S. Middleton, H.S. Viswanathan, K.A. Berchtold, R.P. Singh, et al., Greening coal: breakthroughs and challenges in carbon capture and storage, Environ. Sci. Technol. 45 (20) (2011) 8597–8604.
[6] B. Metz, O. Davidson, H. De Coninck, M. Loos, L. Meyer, Carbon dioxide capture and storage, 2005.
[7] E.S. Rubin, C. Chen, A.B. Rao, Cost and performance of fossil fuel power plants with CO_2 capture and storage, Energy Policy 35 (9) (2007) 4444–4454.

[8] J. Gibbins, H. Chalmers, Carbon capture and storage, Energy Policy 36 (12) (2008) 4317–4322.
[9] M.E. Boot-Handford, J.C. Abanades, E.J. Anthony, M.J. Blunt, S. Brandani, N. Mac Dowell, et al., Carbon capture and storage update, Energy Environ. Sci. 7 (1) (2014) 130–189.
[10] S. Choi, J.H. Drese, C.W. Jones, Adsorbent materials for carbon dioxide capture from large anthropogenic point sources, ChemSusChem. 2 (9) (2009) 796–854.
[11] T.C. Drage, C.E. Snape, L.A. Stevens, J. Wood, J. Wang, A.I. Cooper, et al., Materials challenges for the development of solid sorbents for post-combustion carbon capture, J. Mater. Chem. 22 (7) (2012) 2815–2823.
[12] A.S. Bhown, B.C. Freeman, Analysis and status of post-combustion carbon dioxide capture technologies, Environ. Sci. Technol. 45 (20) (2011) 8624–8632.
[13] A. Goeppert, M. Czaun, R.B. May, G.S. Prakash, G.A. Olah, S. Narayanan, Carbon dioxide capture from the air using a polyamine based regenerable solid adsorbent, J. Am. Chem. Soc. 133 (50) (2011) 20164–20167.
[14] J.-R. Li, Y. Ma, M.C. McCarthy, J. Sculley, J. Yu, H.-K. Jeong, et al., Carbon dioxide capture-related gas adsorption and separation in metal-organic frameworks, Coord. Chem. Rev. 255 (15) (2011) 1791–1823.
[15] N.R. Stuckert, R.T. Yang, CO_2 capture from the atmosphere and simultaneous concentration using zeolites and amine-grafted SBA-15, Environ. Sci. Technol. 45 (23) (2011) 10257–10264.
[16] K. Sumida, D.L. Rogow, J.A. Mason, T.M. McDonald, E.D. Bloch, Z.R. Herm, et al., Carbon dioxide capture in metal-organic frameworks, Chem. Rev. 112 (2) (2011) 724–781.
[17] L.K. de Souza, N.P. Wickramaratne, A.S. Ello, M.J. Costa, C.E. da Costa, M. Jaroniec, Enhancement of CO_2 adsorption on phenolic resin-based mesoporous carbons by KOH activation, Carbon 65 (2013) 334–340.
[18] Y.C. Park, S.-H. Jo, C.K. Ryu, C.-K. Yi, Demonstration of pilot scale carbon dioxide capture system using dry regenerable sorbents to the real coal-fired power plant in Korea, Energy Procedia 4 (2011) 1508–1512.
[19] J. Wang, S. Kaskel, KOH activation of carbon-based materials for energy storage, J. Mater. Chem. 22 (45) (2012) 23710–23725.
[20] C. Pevida, T. Drage, C.E. Snape, Silica-templated melamine-formaldehyde resin derived adsorbents for CO_2 capture, Carbon 46 (11) (2008) 1464–1474.
[21] Y. Juan, Q. Ke-qiang, Preparation of activated carbon by chemical activation under vacuum, Environ. Sci. Technol. 43 (9) (2009) 3385–3390.
[22] C. Pevida, M. Plaza, B. Arias, J. Fermoso, F. Rubiera, J. Pis, Surface modification of activated carbons for CO_2 capture, Appl. Surf. Sci. 254 (22) (2008) 7165–7172.
[23] J. Figueiredo, M. Pereira, M. Freitas, J. Orfao, Modification of the surface chemistry of activated carbons, Carbon 37 (9) (1999) 1379–1389.
[24] P. Chingombe, B. Saha, R. Wakeman, Surface modification and characterisation of a coal-based activated carbon, Carbon 43 (15) (2005) 3132–3143.
[25] M.S. Shafeeyan, W.M.A.W. Daud, A. Houshmand, A. Shamiri, A review on surface modification of activated carbon for carbon dioxide adsorption, J. Anal. Appl. Pyrol. 89 (2) (2010) 143–151.
[26] F. Rodriguez-Reinoso, M. Molina-Sabio, Activated carbons from lignocellulosic materials by chemical and/or physical activation: an overview, Carbon 30 (7) (1992) 1111–1118.
[27] D. Vargas, L. Giraldo, A. Erto, J. Moreno-Piraján, Chemical modification of activated carbon monoliths for CO_2 adsorption, J. Therm. Anal. Calorim. 114 (3) (2013) 1039–1047.
[28] A. Erto, A. Silvestre-Albero, J. Silvestre-Albero, F. Rodríguez-Reinoso, M. Balsamo, A. Lancia, et al., Carbon-supported ionic liquids as innovative adsorbents for CO_2 separation from synthetic flue-gas, J. Colloid Interface Sci. 448 (2015) 41–50.
[29] F. Montagnaro, A. Silvestre-Albero, J. Silvestre-Albero, F. Rodríguez-Reinoso, A. Erto, A. Lancia, et al., Post-combustion CO_2 adsorption on activated carbons with different textural properties, Microporous Mesoporous Mater. (2014).
[30] A. Wahby, J. Silvestre-Albero, A. Sepúlveda-Escribano, F. Rodríguez-Reinoso, CO_2 adsorption on carbon molecular sieves, Microporous Mesoporous Mater. 164 (2012) 280–287.
[31] Y. Liu, J. Wilcox, Effects of surface heterogeneity on the adsorption of $_{CO2}$ in microporous carbons, Environ. Sci. Technol. 46 (3) (2012) 1940–1947.
[32] J. Silvestre-Albero, A. Wahby, A. Sepúlveda-Escribano, M. Martínez-Escandell, K. Kaneko, F. Rodríguez-Reinoso, Ultrahigh CO_2 adsorption capacity on carbon molecular sieves at room temperature, Chem. Commun. 47 (24) (2011) 6840–6842.
[33] J. Wang, A. Heerwig, M.R. Lohe, M. Oschatz, L. Borchardt, S. Kaskel, Fungi-based porous carbons for CO_2 adsorption and separation, J. Mater. Chem. 22 (28) (2012) 13911–13913.
[34] Y. Xia, R. Mokaya, G.S. Walker, Y. Zhu, Superior CO_2 adsorption capacity on N-doped, high-surface-area, microporous carbons templated from zeolite, Adv. Energy Mater. 1 (4) (2011) 678–683.
[35] L. Zhao, L.Z. Fan, M.Q. Zhou, H. Guan, S. Qiao, M. Antonietti, et al., Nitrogen-containing hydrothermal carbons with superior performance in supercapacitors, Adv. Mater. 22 (45) (2010) 5202–5206.
[36] Y. Zhao, X. Liu, K.X. Yao, L. Zhao, Y. Han, Superior capture of CO_2 achieved by introducing extra-framework cations into N-doped microporous carbon, Chem. Mater. 24 (24) (2012) 4725–4734.
[37] B. Zhu, K. Li, J. Liu, H. Liu, C. Sun, C.E. Snape, et al., Nitrogen-enriched and hierarchically porous carbon macro-spheres–ideal for large-scale CO_2 capture, J. Mater. Chem. A 2 (15) (2014) 5481–5489.
[38] D. Lozano-Castello, M. Lillo-Rodenas, D. Cazorla-Amoros, A. Linares-Solano, Preparation of activated carbons from Spanish anthracite: I. Activation by KOH, Carbon 39 (5) (2001) 741–749.
[39] V. Presser, J. McDonough, S.-H. Yeon, Y. Gogotsi, Effect of pore size on carbon dioxide sorption by carbide derived carbon, Energy Environ. Sci. 4 (8) (2011) 3059–3066.
[40] M. Sevilla, P. Valle-Vigón, A.B. Fuertes, N-doped polypyrrole-based porous carbons for CO_2 capture, Adv. Funct. Mater. 21 (14) (2011) 2781–2787.
[41] S.-H. Yoon, S. Lim, Y. Song, Y. Ota, W. Qiao, A. Tanaka, et al., KOH activation of carbon nanofibers, Carbon 42 (8) (2004) 1723–1729.
[42] N. Sun, C. Sun, H. Liu, J. Liu, L. Stevens, T. Drage, et al., Synthesis, characterization and evaluation of activated spherical carbon materials for CO_2 capture, Fuel 113 (2013) 854–862.
[43] E.S. Kikkinides, R.T. Yang, S.H. Cho, Concentration and recovery of carbon dioxide from flue gas by pressure swing adsorption, Ind. Eng. Chem. Res. 32 (11) (1993) 2714–2720.
[44] S. Himeno, T. Komatsu, S. Fujita, High-pressure adsorption equilibria of methane and carbon dioxide on several activated carbons, J. Chem. Eng. Data 50 (2) (2005) 369–376.
[45] W.R. Alesi, M. Gray, J.R. Kitchin, CO_2 adsorption on supported molecular amidine systems on activated carbon, ChemSusChem. 3 (8) (2010) 948–956.
[46] G.P. Hao, W.C. Li, D. Qian, A.H. Lu, Rapid synthesis of nitrogen-doped porous carbon monolith for CO_2 capture, Adv. Mater. 22 (7) (2010) 853–857.
[47] M. Plaza, C. Pevida, A. Arenillas, F. Rubiera, J. Pis, CO_2 capture by adsorption with nitrogen enriched carbons, Fuel 86 (14) (2007) 2204–2212.
[48] M.S. Shafeeyan, W.M.A.W. Daud, A. Houshmand, A. Arami-Niya, Ammonia modification of activated carbon to enhance carbon dioxide adsorption: effect of pre-oxidation, Appl. Surf. Sci. 257 (9) (2011) 3936–3942.
[49] M.-M. Titirici, Sustainable Carbon Materials from Hydrothermal Processes, Wiley Online Library, 2013.
[50] L.C. Dolores, P.M.L. Juan, C. Falco, M.M. Titirici, C.A. Diego. Porous Biomass-Derived Carbons: Activated Carbons. Sustainable Carbon Materials from Hydrothermal Processes, 2013, pp. 75–100.
[51] V. Verheyen, R. Rathbone, M. Jagtoyen, F. Derbyshire, Activated extrudates by oxidation and KOH activation of bituminous coal, Carbon 33 (6) (1995) 763–772.
[52] J.B. Parra Soto, J. De Sousa, R.C. Bansal, J. Pis Martínez, Characterization of activated carbons by the BET equation: an alternative approach, Adsorpt. Sci. Technol. 12 (1) (1995) 51–66.
[53] K.S. Sing, Reporting physisorption data for gas/solid systems with special reference to the determination of surface area and porosity (Recommendations 1984), Pure Appl. Chem. 57 (4) (1985) 603–619.
[54] A. Oya, S. Yoshida, J. Alcaniz-Monge, A. Linares-Solano, Formation of mesopores in phenolic resin-derived carbon fiber by catalytic activation using cobalt, Carbon 33 (8) (1995) 1085–1090.
[55] S.R. Tennison, Phenolic-resin-derived activated carbons, Appl. Catal. A 173 (2) (1998) 289–311.
[56] M. Lillo-Ródenas, D. Cazorla-Amorós, A. Linares-Solano, Understanding chemical reactions between carbons and NaOH and KOH: an insight into the chemical activation mechanism, Carbon 41 (2) (2003) 267–275.
[57] E. Raymundo-Piñero, P. Azaïs, T. Cacciaguerra, D. Cazorla-Amorós, A. Linares-Solano, F. Béguin, KOH and NaOH activation mechanisms of multiwalled carbon nanotubes with different structural organisation, Carbon 43 (4) (2005) 786–795.
[58] J. Romanos, M. Beckner, T. Rash, L. Firlej, B. Kuchta, P. Yu, et al., Nanospace engineering of KOH activated carbon, Nanotechnology 23 (1) (2012) 015401.
[59] P.I. Neel, B. Viswanathan, T. Varadarajan, Methods of activation and specific applications of carbon materials, 2009.
[60] D. Lozano-Castello, J. Calo, D. Cazorla-Amoros, A. Linares-Solano, Carbon activation with KOH as explored by temperature programmed techniques, and the effects of hydrogen, Carbon 45 (13) (2007) 2529–2536.
[61] T. Otowa, R. Tanibata, M. Itoh, Production and adsorption characteristics of MAXSORB: high-surface-area active carbon, Gas Sep. Purif. 7 (4) (1993) 241–245.
[62] A. Ahmadpour, D. Do, The preparation of activated carbon from macadamia nutshell by chemical activation, Carbon 35 (12) (1997) 1723–1732.
[63] K. Kierzek, E. Frackowiak, G. Lota, G. Gryglewicz, J. Machnikowski, Electrochemical capacitors based on highly porous carbons prepared by KOH activation, Electrochim. Acta 49 (4) (2004) 515–523.
[64] N.P. Wickramaratne, M. Jaroniec, Importance of small micropores in CO_2 capture by phenolic resin-based activated carbon spheres, J. Mater. Chem. A 1 (1) (2013) 112–116.
[65] Y. Zhu, S. Murali, M.D. Stoller, K. Ganesh, W. Cai, P.J. Ferreira, et al., Carbon-based supercapacitors produced by activation of graphene, Science 332 (6037) (2011) 1537–1541.
[66] R. Krishna, Adsorptive separation of $CO_2/CH_4/CO$ gas mixtures at high pressures, Microporous Mesoporous Mater. 156 (2012) 217–223.
[67] A. Myers, P. Monson, Adsorption in porous materials at high pressure: theory and experiment, Langmuir 18 (26) (2002) 10261–10273.
[68] D.B. Robinson, D.-Y. Peng, S.Y. Chung, The development of the Peng–Robinson equation and its application to phase equilibrium in a system containing methanol, Fluid Phase Equilib. 24 (1) (1985) 25–41.
[69] D.B. Robinson, D.-Y. Peng, The Characterization of the Heptanes and Heavier Fractions for the GPA Peng-Robinson Programs, Gas Processors Association, 1978.
[70] Y. Zhao, L. Zhao, K.X. Yao, Y. Yang, Q. Zhang, Y. Han, Novel porous carbon materials with ultrahigh nitrogen contents for selective CO_2 capture, J. Mater. Chem. 22 (37) (2012) 19726–19731.

[71] W. Zhang, H. Liu, C. Sun, T.C. Drage, C.E. Snape, Performance of polyethyleneimine–silica adsorbent for post-combustion CO_2 capture in a bubbling fluidized bed, Chem. Eng. J. 251 (2014) 293–303.
[72] J.A. Mason, K. Sumida, Z.R. Herm, R. Krishna, J.R. Long, Evaluating metal–organic frameworks for post-combustion carbon dioxide capture via temperature swing adsorption, Energy Environ. Sci. 4 (8) (2011) 3030–3040.
[73] Z.R. Herm, R. Krishna, J.R. Long, CO_2/CH_4, CH_4/H_2 and $CO_2/CH_4/H_2$ separations at high pressures using Mg2(dobdc), Microporous Mesoporous Mater. 151 (2012) 481–487.
[74] T. Ben, Y. Li, L. Zhu, D. Zhang, D. Cao, Z. Xiang, et al., Selective adsorption of carbon dioxide by carbonized porous aromatic framework (PAF), Energy Environ. Sci. 5 (8) (2012) 8370–8376.
[75] S.M. Mahurin, J. Gorka, K.M. Nelson, R.T. Mayes, S. Dai, Enhanced CO_2/N_2 selectivity in amidoxime-modified porous carbon, Carbon 67 (2014) 457–464.
[76] W. Lu, J.P. Sculley, D. Yuan, R. Krishna, H.-C. Zhou, Carbon dioxide capture from air using amine-grafted porous polymer networks, J. Phys. Chem. C 117 (8) (2013) 4057–4061.
[77] T.M. McDonald, D.M. D'Alessandro, R. Krishna, J.R. Long, Enhanced carbon dioxide capture upon incorporation of N, *N′*-dimethylethylenediamine in the metal-organic framework CuBTTri, Chem. Sci. 2 (10) (2011) 2022–2028.
[78] P.M. Mathias, R. Kumar, J.D. Moyer, J.M. Schork, S.R. Srinivasan, S.R. Auvil, et al., Correlation of multicomponent gas adsorption by the dual-site Langmuir model. Application to nitrogen/oxygen adsorption on 5A-zeolite, Ind. Eng. Chem. Res. 35 (7) (1996) 2477–2483.
[79] R.C. Bansal, M. Goyal, Activated carbon adsorption, CRC Press, 2010.
[80] C. Shen, C.A. Grande, P. Li, J. Yu, A.E. Rodrigues, Adsorption equilibria and kinetics of CO_2 and N_2 on activated carbon beads, Chem. Eng. J. 160 (2) (2010) 398–407.
[81] M. Bülow, D. Shen, S. Jale, Measurement of sorption equilibria under isosteric conditions: the principles, advantages and limitations, Appl. Surf. Sci. 196 (1) (2002) 157–172.
[82] M.J. Bleda-Martínez, J.A. Maciá-Agulló, D. Lozano-Castelló, E. Morallón, D. Cazorla-Amorós, A. Linares-Solano, Role of surface chemistry on electric double layer capacitance of carbon materials, Carbon 43 (13) (2005) 2677–2684.
[83] A. Pandolfo, A. Hollenkamp, Carbon properties and their role in supercapacitors, J. Power Sources 157 (1) (2006) 11–27.
[84] E. Frackowiak, Carbon materials for supercapacitor application, Phys. Chem. Chem. Phys. 9 (15) (2007) 1774–1785.
[85] T.C. Drage, J.M. Blackman, C. Pevida, C.E. Snape, Evaluation of activated carbon adsorbents for CO_2 capture in gasification, Energy Fuels 23 (5) (2009) 2790–2796.
[86] J. Liu, P.K. Thallapally, B.P. McGrail, D.R. Brown, J. Liu, Progress in adsorption-based CO_2 capture by metal-organic frameworks, Chem. Soc. Rev. 41 (6) (2012) 2308–2322.
[87] A. Martin-Calvo, J.B. Parra, C. Ania, S. Calero, Insights on the anomalous adsorption of carbon dioxide in LTA zeolites, J. Phys. Chem. C 118 (44) (2014) 25460–25467.
[88] S.C. Lee, H.J. Chae, S.J. Lee, B.Y. Choi, C.K. Yi, J.B. Lee, et al., Development of regenerable MgO-based sorbent promoted with K_2CO_3 for CO_2 capture at low temperatures, Environ. Sci. Technol. 42 (8) (2008) 2736–2741.
[89] W. Zhang, H. Liu, C. Sun, T.C. Drage, C.E. Snape, Capturing CO_2 from ambient air using a polyethyleneimine–silica adsorbent in fluidized beds, Chem. Eng. Sci. 116 (2014) 306–316.
[90] S. Sjostrom, H. Krutka, Evaluation of solid sorbents as a retrofit technology for CO_2 capture, Fuel 89 (6) (2010) 1298–1306.
[91] M. Gray, J. Hoffman, D. Hreha, D. Fauth, S. Hedges, K. Champagne, et al., Parametric study of solid amine sorbents for the capture of carbon dioxide, Energy Fuels 23 (10) (2009) 4840–4844.
[92] A. Ebner, M. Gray, N. Chisholm, Q. Black, D. Mumford, M. Nicholson, et al., Suitability of a solid amine sorbent for CO_2 capture by pressure swing adsorption, Ind. Eng. Chem. Res. 50 (9) (2011) 5634–5641.